Microstructure of Ferroelectric Domains in $BaTiO_3$ Observed via X-Ray Microdiffraction

M. Holt,[1,*] Kh. Hassani,[1] and M. Sutton[1,†]

[1]*Physics Department, McGill University, Montreal, Quebec, Canada H3A 2T8*

(Received 2 March 2005; published 19 August 2005)

X-ray microdiffraction utilizing Fresnel zone plate focusing optics has been used to study microstructural properties of individual 90° ferroelectric domains in $BaTiO_3$. Diffraction measurements at a microfocused spot resolution of 0.3 μm over domain widths of $\sim$10 μm unambiguously reveal features of lattice buckling, rotation, and strain near domain boundaries. Our results may be understood within the context of bound residual strain due to lattice mismatch and elastic interactions between neighboring domains.

DOI: 10.1103/PhysRevLett.95.085504 PACS numbers: 62.20.−x, 61.10.−i

Ferroelectric ceramics such as $BaTiO_3$ have been widely studied in recent years, in large part due to the possibility of novel applications in nonlinear optics, as nonvolatile memory storage devices, and most recently as material for highly polarized nanosystems of reduced dimensionality [1,2]. While in principle these materials are good candidates for device purposes, progress has been limited by technical challenges such as crystal failure and switching fatigue, indicating a fundamentally insufficient understanding of domain microcharacteristics and response [3,4]. The future success of these applications will relate to our understanding of the micromechanical properties, interactions, and underlying structure of ferroelectric domains.

As nearly all interesting macrostructural properties of ferroelectric materials are governed by their microstructural characteristics, ferroelectric domains have been the subject of wide-ranging experimental and theoretical study [1–10]. These domains can be spatially imaged by various techniques such as scanning microscopy [5–7], optical techniques [8], and x-ray topography [9]. These methods can be applied at exceptionally high spatial resolutions, but provide only limited quantitative information on internal stress, strain states, and lattice rotation interior to domains. This is important information since dynamic properties, such as polarization switching by external fields, are strongly affected by the micromechanics of single domains. X-ray microdiffraction is best suited to answer these questions as it resolves lattice orientation, strain, and buckling on a length scale interior to a single domain. Previous x-ray work [10] using a scanning reflection Laue geometry was performed at an insufficient spatial resolution ($\sim$3 μm) to observe the features we now report. The use of Fresnel zone plate optics [11] allows this study to establish a microfocused monochromatic x-ray beam spot of smallest dimension 0.3 μm (for comparison domain widths in zero-field-cooled (ZFC) $BaTiO_3$ are typically $\sim$10 μm). Domain microstructure information can then be obtained by scanning the diffraction measurements as a function of sample position.

Barium titanate [12] is characterized by a cubic-to-tetragonal structural phase transition at the Curie temperature ($T_C = 120\,^\circ$C) associated with a small axial displacement of the central titanium atom at temperatures below T_C. This distortion introduces a dipole moment to each unit cell, and the now tetragonal crystal seeks to minimize electrostatic and mechanical stress by the formation of ferroelectric domains. When undergoing the phase transition, each unit cell has a sixfold choice of dipole axis, possibly leading to multiple ferroelectric domains. We exclusively discuss 90° domains typically present in $BaTiO_3$ that alternate **a**-**c**-**a** dipole moments parallel and perpendicular to the surface normal (Fig. 1). For the [100] orientation of $BaTiO_3$ these domain boundaries fall away from the surface at approximately 45° to the surface normal. This geometry establishes an asymmetry between the interface, which lies below its neighbor, having an angle of $\sim$135° with respect to the surface and the interface lying above its neighboring domain having an angle of $\sim$45°.

Our experiment was performed at the 8-ID-E side station of IMM/XOR-CAT (IBM, MIT, McGill, X-ray Operations,

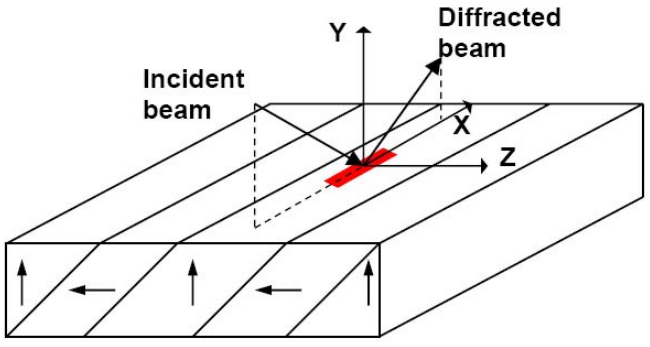

FIG. 1 (color online). Ferroelectric 90° domain walls found in ferroelectric $BaTiO_3$. For the [100] oriented crystal the domain boundaries fall away at 45° to the surface normal. The scattering geometry and microfocused spot on the sample are indicated. As the microdiffracted x-ray scattering volume is moved relative to the sample (along **z**), diffracted intensity is collected from both the (002) and the (200) reflections.

and Research Collaborative Access Team) at the Advanced Photon Source, Argonne National Laboratory. The 8-ID undulator beam line specializes in coherent diffraction, and, although coherence is not used in this measurement, the overall goal of this station is to provide time-resolved coherent microdiffraction measurements of systems of interest to materials studies. A Fresnel zone plate (250 μm diameter at 37 cm focal length) was employed to focus 7.5 keV x rays achieving a diffraction-limited focused spot of dimensions 0.3 μm $\times$ 3 μm (vertical by horizontal) with an efficiency of $\sim$30% of the illuminated flux [11]. This spot is diffraction limited in the vertical. For this measurement the long dimension of the beam spot was aligned to be parallel to the domain walls, giving the best spatial resolution across the wall. Sample positioning used an encoded XYZ translation stage with $\sim$50 nm step size over a 25 mm range of motion. Both the focused spot and translation system are integrated into the center of rotation of a three circle diffractometer, enabling microdiffraction measurements with a high degree of precision and efficiency. We label the three diffraction angles 2θ (detector angle), θ (in plane angle), and χ (out of plane angle). X rays were detected by a high resolution area detector with $\sim$1.5 μm pixels. This consisted of a CCD on a microscope looking at an x-ray scintillator placed at $\sim$30 cm from the sample.

At each sample position the three diffraction angles are scanned, and the results are summarized in Figs. 2 and 3. The measurements taken at the domain centers are used to represent the reference position of each domain. The 2θ scans correspond to lattice constants of $a = 3.992$ Å and $c = 4.036$ Å. Orientation is preserved from **c** domain to **c** domain (and from **a** domain to **a** domain) over many sets of domain walls to better than 0.001°. The relative position of the (002) and (200) peaks measures the angle between **a** and **c** domains as 89.35°. As two crystallites with a tetragonal lattice are perfectly matched along a domain wall with an angle $\arctan(\mathbf{a}/\mathbf{c}) = 44.685°$ [12], we expect an angle between these domains of 89.37° $\pm$ 0.01°. Any deviation from this angle contributes to a strain at the interface to be further discussed below.

Integrated intensity from the (002) reflection as a function of sample position at a step size of 0.5 μm is shown in Fig. 2(a). Regions of high (or low) intensity correspond to the ferro-distorted **c** axis being oriented parallel (or orthogonal) to the surface normal. Evident in this image is a periodic 90° rotation of the ferroelectric axis with domain width $\sim$10 μm. This region is representative of the majority of the crystal's surface. For each sample position (pixel), data can be collected on both the (002) and the (200) (**c**-axis and **a**-axis) diffraction peaks, and the intensity of both peaks along a line from the center of this image is shown in detail in Fig. 2(b). In the case of [001] oriented $BaTiO_3$, the approximately 45° domain walls should give an overlapping region of $\sim$5 μm where both domains are within an absorption length of the surface.

Note a small, but consistent, asymmetry is seen in the low intensity line shapes of each curve in Fig. 2(b); the intensity increases on the left-hand side of each peak in an exponential fashion and falls to zero in a steeper, more linear fashion. This is due to the domain geometry that

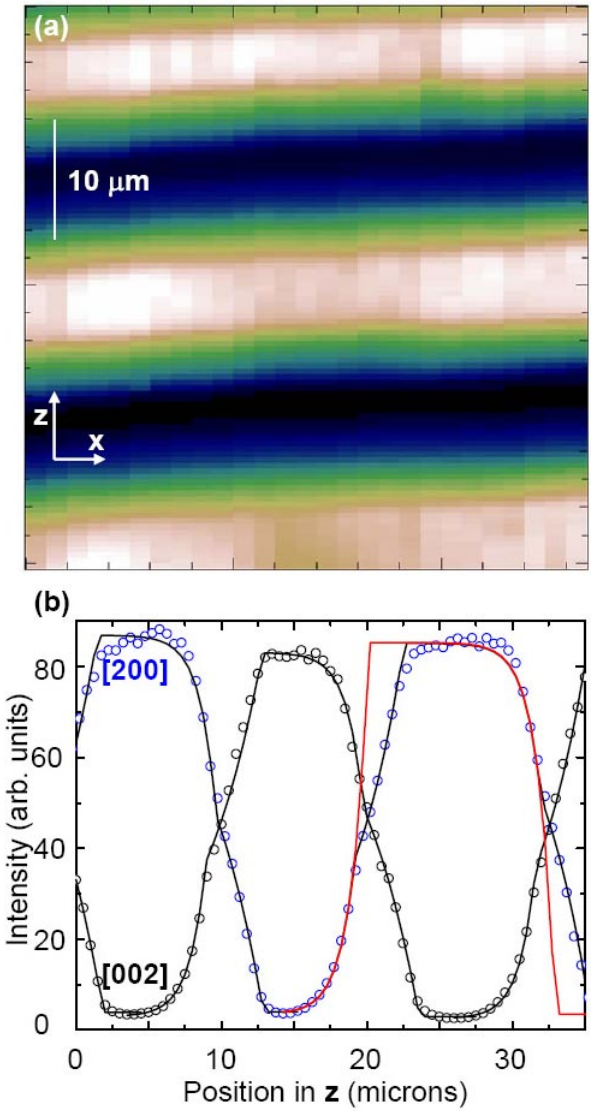

FIG. 2 (color online). Integrated microdiffracted x-ray intensity from $BaTiO_3$ ferroelectric domains taken as a function of sample position. (a) A map of the (002) diffraction peak intensity from a 50 μm $\times$ 50 μm region at 0.5 μm steps. The periodic domain structure in the **z** direction is clearly evident as the **c** axis undergoes 90° rotations at $\sim$10 μm intervals. (b) An overlay plot of integrated intensity from both (002) and (200) domains. The registry of these scans shows the alternating **c**-axis–**a**-axis–**c**-axis pattern. At each point complete crystallographic data were recorded for both the (002) and the (200) diffraction peaks—this specifies lattice rotation and expansion along the surface normal in both domains. The solid black lines are a two-component model of the active scattering volume following Fig. 3(c). A single component model shown by the red line is inadequate to describe the data.

determines scattering volume, and the integrated intensity can then be represented by a simple absorption model

$$I_{\text{integrated}}(\mathbf{z}) \propto e^{-2a(\mathbf{z})/\lambda \sin(\Theta)}(1 - e^{-2[b(\mathbf{z})-a(\mathbf{z})]/\lambda \sin(\Theta)}). \quad (1)$$

In this equation λ is the attenuation length of $BaTiO_3$ (5.4 μm at 7.5 keV), θ is the scattering angle ($\sim 24°$), and $a(\mathbf{z})$ and $b(\mathbf{z})$ are linear functions that specify the upper and lower domain boundary depths (here all domains have the same profile). The observed "kinks" in our intensity data (at positions 10, 20, 35 μm) cannot be adequately explained by a simple straight-line model of the domain walls [the red line in Fig. 2(b)]. This indicates that the domain boundary function deviates from its expected straight-line $\sim 45°$ value at points near the surface. A simple extension of this model, which has two linear components and assigns the near-surface domain wall a different angle, results in a greatly improved fit [the black line in Figs. 2(b) and 3(b)]. It is important to note that domain strain and rotation mainly affect the width and position of this rocking curve, whereas the total integrated intensity following Eq. (1) can be taken as a direct measure of the active scattering volume. This model estimates the depth of the domain walls, giving an unambiguous reference point for where the domain wall intersects the surface. For the fit in Fig. 2(b) the depth of the crossover point in all domains is 1 μm, and the domain walls intercept the surface at positions 10, 20, and 35 μm with an angle of 20°. We have performed microdiffraction scans over many regions of the crystal and always see this asymmetry. Presumably, this structure reflects some minimization of energies at the near-surface domain walls.

Figure 3 summarizes the diffraction data taken over a single 90° ferroelectric domain in $BaTiO_3$. The implications of these data are discussed in more detail below. The integrated rocking curve intensity of the (002) reflection is shown in Fig. 3(b), where the black line is a theoretical result following Eq. (1). The parameters of this fit help us to draw the blue (dotted) and red (solid) lines on this and all subsequent panels. For each domain wall, the domain-surface interface is given by the solid line, and the point at which the domain boundary is beyond one attenuation length (and so contributes less than 10% to the intensity) is given by the dotted line [$\lambda \sin(\theta) \sim 2.5$ μm]. Figure 3(c) describes the relative lattice strain ($\Delta c/c$) along the surface normal directly resulting from the diffraction peak 2Θ value. The lattice constant measured at $\mathbf{z} = -15$ μm is used as the reference—this represents the measured lattice constant of the parts of the domain farthest from the surface. The near-surface lattice experiences a small compressive strain at the 135° interface peaking at the inflection point, is constant but slightly compressive through the domain interior, and exhibits a larger expansive strain leading up to the 45° interface again peaking at the surface-bulk inflection point. The integrated intensity profile shown in Fig. 3(b) maps the active [002] scattering volume as a function of $\mathbf{z}$ as shown in Fig. 3(a). Note that the points where the domain walls change direction near the surface are points associated with the most lattice strain and rotation within the domain. These strain maxima and minima are also associated with lattice rotations leading up to and away from the critical points. The c-axis lattice vector undergoes rotation in θ and χ near the boundary regions, as shown in Figs. 3(e) and 3(f). Note that the lattice rotations in both orthogonal senses do not exactly match in $\mathbf{z}$ position with the strain critical points but instead are offset by about ~ 2 μm from the strain maximum or minimum and have opposite directions on each side of the domain. This is most clearly seen when compar-

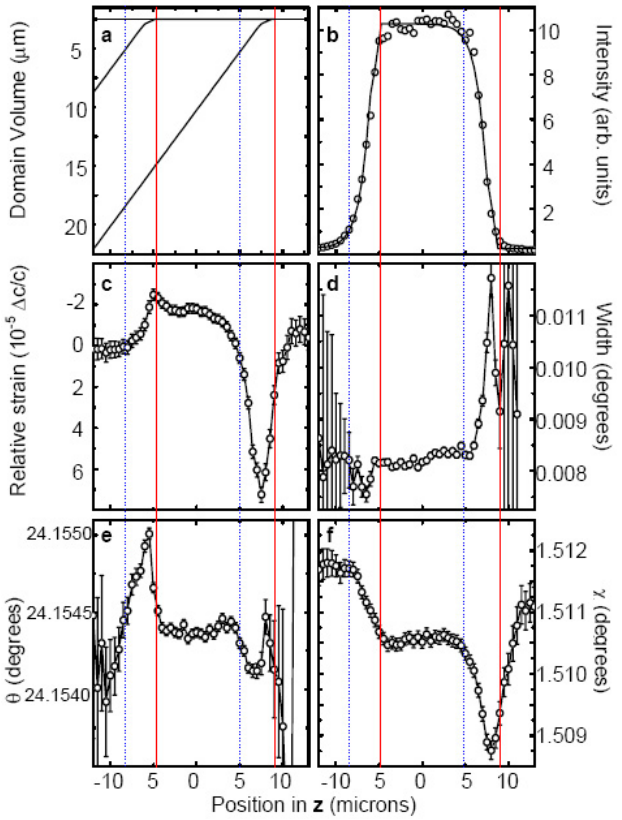

FIG. 3 (color online). This figure is a summary of detailed crystallographic data taken on the (002) reflection as a function of beam spot position across a single $BaTiO_3$ domain. Two approximate reference points are marked in all panels—the intersection of domain walls with one x-ray attenuation length from the surface (dotted blue line), and the surface–domain wall intersection (solid red line). (a) A schematic showing the active diffracting volume (domain boundary positions and pitch) resulting from our two-component fit. (b) Integrated intensity of the rocking curve. (c) The relative strain along the surface normal mapped directly from the 2Θ position of the [002] peak. (d) The rocking curve width in θ diverges as the scattering volume approaches zero. (e),(f) The lattice vector exhibits a marked rotation in θ (e) and χ (f) about points of strain maxima and minima [compare to Fig. 3(b)].

ing the θ rotation Fig. 3(e) with the strain curve in Fig. 3(c). Figure 3(d) shows that the peak width is sharpest at the 135° interface and diverges towards the 45° interface. This is expected as both strain broadening and the finite size of the scattering volume affect the rocking curve width at this interface.

From our data it is clear that the domain wall is not a flat planar object, nor is it locked to the crystal axes. These features are not considered in the many papers that calculate domain wall profiles [13,14]. As the lattice is tetragonal, there is a lattice mismatch along the surface normal between neighboring **c**-axis and **a**-axis domains (Fig. 1). As discussed above, as the crystal is not in the strain-free rotation state there is a slight compensatory strain of the lattice. One explanation of such a rotation is proposed by Meyer and Vanderbilt [15], who suggest the presence of an induced dipole layer at the domain boundary produces such a rotation. Such a mechanism would lead to a strain profile across the domain interior as it accommodates both its neighbors [16]. One must also account for domain-domain interactions. The formation of a 90° domain structure minimizes total elastic strain of the crystal at the expense of domain wall energy [17]. It is expected that long-range elastic interactions between domains play a dominant role in observed morphology, and in essence each domain can be viewed as a clamped crystallite in competition with its neighbors [14]. Importantly for our case, these elastic stresses are inherently asymmetric within a near-surface region due to a 45° surface truncation of the domain boundaries. That is, the thin ~45° wedge should be more distorted by its neighbors than the ~135° corner. Consequently, the ''beneath'' interface (135°) and the near-surface domain interior respond to elastic stress in an opposite sense relative to the ''above'' interface (45°). From these considerations, we expect any domain-domain elastic strain to appear as small signatures located near the boundary-surface interfaces with the 135° boundary and the near-surface domain interior stressed in an opposite sense to the 45° boundary and the buried bulk interfaces. As shown in Fig. 3(b), all these qualitative features are experimentally observed in 90° ZFC domains of $BaTiO_3$.

In conclusion, we have observed microstrain signatures and lattice rotations within single ferroelectric domains of $BaTiO_3$. The nominal 45° walls between **a** and **c** domains become ~20° within about 1 μm of the surface. Besides the expected symmetric strain of the domain interior due to lattice mismatch [16], an additional asymmetric contribution occurs near the points where the domain boundaries intersect the surface. For the first time, features of ferroelectric domain micromechanics in $BaTiO_3$ have been unambiguously observed on a submicron length scale using x-ray microdiffraction. Research into the dynamic response of domain microstructure to external field, stress, and temperature is ongoing. These and future results will help elucidate nonequilibrium micromechanics and directly impact our quest for modern functional materials.

Use of the Advanced Photon Source was supported by the U.S. Department of Energy, Office of Science, Office of Basic Energy Sciences, under Contract No. W-31-109-Eng-38.

*Present address: X-ray Microscopy Group, Center for Nanoscale Materials, Advanced Photon Source, Argonne, IL, USA.

†To whom correspondence should be addressed. Electronic address: mark@physics.mcgill.ca

[1] W. J. Merz, Phys. Rev. **95**, 690 (1954).
[2] Y. Luo *et al.*, Appl. Phys. Lett. **83**, 440 (2003).
[3] E. Burcsu, G. Ravichandran, and K. Bhattacharya, Appl. Phys. Lett. **77**, 1698 (2000).
[4] D. Damjanovic, Rep. Prog. Phys. **61**, 1267 (1998).
[5] S. V. Kalinin, C. Y. Johnson, and D. A. Bonnell, J. Appl. Phys. **91**, 3816 (2002).
[6] J. Munoz-Saldana, G. A. Schneider, and L. M. Eng, Surf. Sci. **480**, L402 (2001).
[7] V. Likodimos, X. K. Orlik, L. Pardi, M. Labardi, and M. Allegrini, J. Appl. Phys. **87**, 443 (2000).
[8] T. J. Yang, B. Gopalan, P. J. Swart, and U. Mohideen, Phys. Rev. Lett. **82**, 4106 (1999).
[9] Y. Yoneda, Y. Kohmura, Y. Suzuki, S. Hamazaki, and M. Takashige, J. Phys. Soc. Jpn. **73**, 1050 (2004).
[10] R. C. Rogan, N. Tamura, G. A. Swift, and E. Ustundag, Nat. Mater. **2**, 379 (2003).
[11] B. Lai. *et al.*, Appl. Phys. Lett. **61**, 1877 (1992).
[12] Our crystal was purchased from MTI Corporation, Richmond, CA. We ordered a [001] oriented single crystal with both sides polished—there was no other sample preparation.
[13] A. Y. Emelyanov, N. A. Pertsev, and E. K. H. Salje, J. Appl. Phys. **89**, 1355 (2001).
[14] S. Nambu and D. A. Sagala, Phys. Rev. B **50**, 5838 (1994).
[15] B. Meyer and D. Vanderbilt, Phys. Rev. B **65**, 104111 (2002).
[16] N. Floquet *et al.*, J. Phys. III (France) **7**, 1105 (1997).
[17] E. K. W. Goo, R. K. Mishra, and G. Thomas, J. Appl. Phys. **52**, 2940 (1981).